HHS Public Access

Author manuscript

Biofabrication. Author manuscript; available in PMC 2016 November 22.

Published in final edited form as:

Biofabrication. ; 8(3): 035012. doi:10.1088/1758-5090/8/3/035012.

Differences in time-dependent mechanical properties between extruded and molded hydrogels

N Ersumo, **CE Witherel**, and **KL Spiller**

School of Biomedical Engineering, Science & Health Systems, Drexel University, PA19104, USA

KL Spiller: spiller@drexel.edu

Abstract

The mechanical properties of hydrogels used in biomaterials and tissue engineering applications are critical determinants of their functionality. Despite the recent rise of additive manufacturing, and specifically extrusion-based bioprinting, as a prominent biofabrication method, comprehensive studies investigating the mechanical behavior of extruded constructs remain lacking. To address this gap in knowledge, we compared the mechanical properties and swelling properties of crosslinked gelatin-based hydrogels prepared by conventional molding techniques or by 3D bioprinting using a BioBots Beta pneumatic extruder. A preliminary characterization of the impact of bioprinting parameters on construct properties revealed that both Young's modulus and optimal extruding pressure increased with polymer content, and that printing resolution increased with both printing speed and nozzle gauge. High viability (>95%) of encapsulated NIH 3T3 fibroblasts confirmed the cytocompatibility of the construct preparation process. Interestingly, the Young's moduli of extruded and molded constructs were not different, but extruded constructs did show increases in both the rate and extent of time-dependent mechanical behavior observed in creep. Despite similar polymer densities, extruded hydrogels showed greater swelling over time compared to molded hydrogels, suggesting that differences in creep behavior derived from differences in microstructure and fluid flow. Because of the crucial roles of time-dependent mechanical properties, fluid flow, and swelling properties on tissue and cell behavior, these findings highlight the need for greater consideration of the effects of the extrusion process on hydrogel properties.

Keywords

bioprinting; hydrogels; extrusion; time-dependent; mechanical properties

1. Introduction

In recent years, the increasingly apparent shortage of organs for transplantation [1] has prompted the rise of novel tissue engineering approaches. Hydrogels are particularly useful biomaterials for biomedical applications because their mechanical behavior mimics that of native tissue extracellular matrix [2]. These cross-linked water-swollen polymer structures possess porous networks that allow nutrient diffusion to encapsulated cells [3], and generate bulk time-dependent poroelastic properties [4, 5]. Furthermore, the polymer networks themselves are capable of rearrangement [6, 7], conferring bulk viscoelastic properties to the

hydrogels and adding yet another dimension of complexity which can be tuned to engineer synthetic tissue.

Additive manufacturing techniques allow for precise spatial control in the fabrication of hydrogel constructs. Indeed, bioprinting, which generates constructs through layer-by-layer deposition of cell-laden hydrogel material, has emerged as an advantageous approach over more traditional methods, such as molding, that do not offer sufficient control over the intricacies associated with engineering complex tissues [8]. In particular, bioprinting has the potential to allow encapsulation and patterning of multiple cell types as well as accurate control over construct geometry at the microenvironmental level. Though current bioprinting approaches include inkjet and laser-assisted printing, extrusion printing has become an appealing option for biofabrication due to its affordability, capacity for high cell density and adaptability for hydrogels with a diverse range of properties (viscosity, gelation method, etc) [9–12].

The versatile nature of extrusion-based bioprinting has elicited a wide-ranging assessment of the cytocompatibility of various biomaterials with respect to specific bioprinting modalities [13]. In order to develop robust, consistent and scalable biofabrication platforms, efforts have also been made to characterize the impact of bioprinting parameters, including printing speed and pressure as well as needle diameter, on extruded construct properties such as resolution [14, 15]. However, investigation into the mechanical behavior of extruded constructs as it compares to conventional biofabrication techniques remains lacking. Indeed, previous mechanical characterization studies of extruded constructs are largely constrained to the elastic component of construct behavior [16–18] and do not extend to evaluating the mechanism behind differences in both elastic and time-dependent mechanical properties resulting from the bioprinting process itself [19]. Another crucial characteristic of hydrogels is their capacity to undergo swelling and shrinking as a result of fluid flow in response to imbalances between osmotic pressure, electrostatic forces and elastic restoring forces [20, 21]. By tuning the characteristics of microporous, macroporous or superporous hydrogels, swelling behavior can be altered to mimic different tissues such as cartilage [22], to develop stimulus-responsive biomaterials for drug delivery [23], and to serve various functions such as preventing post-surgical soft tissue adhesion [24]. However, examination into the impact of extrusion on the swelling behavior of constructs remains limited.

Thus, the objective of this study was to gain a mechanistic understanding of how bioprinting affects the mechanical and swelling properties of extruded hydrogel constructs as part of a characterization evaluating the impact of both hydrogel composition and bioprinting parameters on construct properties. The employed biofabrication platform consists of a Bio-Bots Beta pneumatic extruder in combination with gelatin methacrylate (GelMA) hydrogel (figures 1(a) and (b)). GelMA was chosen because it is a widely used bioink for extrusion [25, 26] that contains cell-binding RGD motifs [27] and supports encapsulated cell viability [18, 28]. We modulated parameters including polymer content, photocrosslinking initiator concentration, printing speed, nozzle inner diameter, and printing pressure (figure 1(c)). Construct quality and resolution were evaluated using optical microscopy. Cell viability of cells encapsulated in extruded and molded constructs was using LIVE/DEAD® staining. Then, hydrogel cylinders of the exact same dimensions (figure 1(d)) were prepared by

molding or extrusion and uniaxial unconfined compression was performed to assess differences in Young's modulus (figure 1(e)). Differences in time-dependent mechanical properties between extruded and molded constructs were subsequently assessed in unconfined creep, an established if preliminary method for the characterization of viscoelastic and poroelastic materials [29–31]. Finally, the mechanism by which extrusion altered the mechanical properties of constructs was examined using optical microscopy and a swelling kinetics study. Taken together, the results of this investigation provide critical information as to how the bioprinting process modulates the performance of extruded constructs under mechanical stimulation. This information will be critical for the development and optimization of bioprinted constructs for *in vitro* tissue engineering and the design of biomaterials that will be undergo mechanical loading *in vivo*.

2. Methods

2.1. Gelatin methacrylation

GelMA was synthesized using previously described methods [25, 26]. Briefly, a 10% w/v solution was prepared by dissolving gelatin (Type A, 300 bloom, porcine skin, Sigma Aldrich) in phosphate buffered saline (PBS) at approximately 60 °C. Following complete dissolution, the solution temperature was maintained at 50 °C and 0.14 ml methacrylic anhydride was added for each gram of dissolved gelatin. The methacrylation reaction was allowed to proceed for 4 h at 50 °C under vigorous stirring. PBS warmed to 40 °C was added to obtain a GelMA concentration of 4.5% w/v, and then ice-cold acetone was added at a volumetric GelMA solution-to-acetone ratio of 1:4, allowing the GelMA to precipitate overnight. The precipitate was dried and dissolved in PBS at a concentration of 10% w/v by heating to approximately 50 °C. Following vacuum filtration through a 0.22 μm filter (polyethersulfone membrane, Fisher Scientific), the solution was dialyzed (Slide-A-Lyzer G2 Dialysis Cassettes, gamma-irradiated, 10 K molecular weight cutoff, Fisher Scientific) for 3 days against deionized water with dialysis media change twice a day. The GelMA solution was finally lyophilized for four days and stored at −20 °C.

2.2. Hydrogel fabrication by bioprinting andmolding

Lithium phenyl-2,4,6-trimethylbenzoylphosphinate (LAP), a cytocompatible photoinitiator activated by visible light at a wavelength of 405 nm [32, 33], was used to initiate photocrosslinking of GelMA. Hydrogels were prepared by dissolving synthesized GelMA at 10–20 w/v% in PBS along with LAP (Biobots) at 0.25% or 0.5%, as indicated. The employed bioprinting system was a BioBots Beta pneumatic extruder, which is equipped with an extrusion pressure range of 0–140 psi and violet light irradiation capability at a wavelength of 405 nm. Prepared hydrogel formulations were loaded in a 10 ml syringe (BD) fitted with 27 gauge (27G, 200 μm inner diameter), 22 gauge (22G, 420 μm inner diameter) or 18 gauge (18G, 840 μm inner diameter) nozzles (Jensen Global Dispensing) for extrusion. Solutions were allowed to physically crosslink (gel) in the syringe prior to extrusion (~20 min). Computer models for the constructs (either lines or cylinders) were designed using Creo Parametric 3.0 and imported into Repetier-Host software, where printing speed was set prior to extrusion. Hydrogel lines were extruded at printing pressures ranging from 60 to 130

psi and travel feed rates from 4 to 12 mm s^{-1}, as indicated, under constant irradiation from the violet light source. Hydrogel cylinders were printed at 100 psi, 8 mm s^{-1}, and in 6 layers.

Molded cylinders of the same dimensions as extruded cylinders were prepared by letting GelMA solutions gelate at solution depths matching that of extruded counterparts for 20 min and then irradiating the solutions under violet light for the same amount of time as extruded cylinders (10 min). Biopsy punches (Fisher Scientific) were subsequently used to obtain molded cylinders with the same dimensions as extruded cylinders (1.4 mm height × 5 mm in diameter), which was confirmed by measuring with calipers. Petri dishes were used as extrusion and molding substrates for extrusion pressure testing, line width evaluation, all mechanical testing and the swelling study, while glass slides were used for the microstructural analysis of constructs with optical microscopy.

2.3. Imaging and analysis for line extrusions and cylinders

Single-layer extruded lines were imaged using an EVOS microscope (transmitted light, phase contrast, 4× magnification). For line extrusions with 18G nozzles, whose widths exceeded the imaging area of the microsope, full-size images of each line were generated by capturing two images spanning the total width and performing a stitching operation using ImageJ [34]. The total area of each line (obtained from ImageJ) was divided by the total length to obtain the average line width.

Representative photographs of extruded and molded cylinders were taken with a Canon S120 digital camera. Using a Zeiss AxioObserver Z1 microscope (phase contrast, 10× magnification), optical micrographs of extruded and molded cylinders (15 mm diameter, 1 mm height) were also taken to assess differences in microstructure. The focal plane of the micrographs was set to the surface of the glass, i.e. the plane of contact between the hydrogel and the glass substrate.

2.4. Cell culture

Although high viability of cells encapsulated in gels prepared with similar crosslinking protocols have been described in several studies [32,33,35], including the use of GelMA, LAP, and light exposure for up to 10 min, we conducted a cell viability assay to assess the impact of the extrusion process on cell viability. NIH/3T3 fibroblasts (ATCC® CRL-1658™) were cultured in Dulbecco's Modified Eagle's Medium (DMEM) with 4.5 g M^{-1} glucose, L-glutamine, and sodium pyruvate (Corning, Corning, NY, Cat. No. 10-013) supplemented with 10% heat-inactivated fetal bovine serum and maintained in an incubator at 37 °C and 5% CO2. Cells were subcultured when approximately 80% confluent and detached using trypsin-EDTA (0.25%, phenol red) (ThermoFisher Scientific, Waltham, MA Cat. No. 25200056). Culture medium was changed every 3–4 days. The baseline viability of the cells was assessed using the Trypan Blue Exclusion method prior to encapsulation and the LIVE/DEAD® assay.

2.5. Cell encapsulation and viability study

Concentrated stock solutions of cells and GelMA (maintained at 37 °C) were gently mixed together resulting in a final concentration of 10% GelMA, 0.25% LAP, and 5.0 × 10 cells

mL^{-1}. For the creation of 3D printed constructs, approximately 5 ml of cell-laden GelMA was poured into a 10 ml syringe and allowed to gel for 20 min, as described above. Next, eight lines were extruded using a 27G nozzle, a travel feed rate of 8 mm s^{-1}, and a layer height of 0.2 mm onto a microscope slide and exposed to 405 nm light for 10 min For the creation of molded hydrogels, 1 ml of cell-laden GelMA was poured into one well of a 6-well plate and allowed to cool for 20 min. The thickness of the hydrogel approximated the thickness of the extruded lines described above. A 5 mm biopsy punch was used to obtain molded hydrogels, which were then were placed on a microscope slide and exposed to 405 nm light for 10 min Cell viability was immediately assessed using the LIVE/DEAD® assay (Thermo Fisher Scientific) according to the manufacturers' instructions. Briefly, the two components were combined with sterile PBS to generate 2 ml of a 4 μm ethidium homodimer (EthD-1) and 2 μm calcein AM solution. Live cells were stained with calcein AM (excitation/emission (ex/em): ~495 nm/~515 nm) and damaged or dead cells were stained with EthD-1 (ex/em: ~495 nm/~635). Hydrogels, encircled with a hydrophobic pen, were incubated with 100–150 μl of LIVE/DEAD® solution for 20 min at room temperature. Cells not subjected to hydrogel encapsulation were used as a positive control.

2.6. Cell-laden hydrogel imaging acquisition and analysis

One image of each sample (n = 5 for all groups: 3D printed, molded, and positive/cell-only control) was immediately captured using confocal microscopy (Zeiss LSM 700, Peabody, MA). A z-stack of images (a minimum of n = 20 per sample), standardized to image through the entire thickness of the sample, was captured through the microscope slides using a resolution of 512 × 512 pixels via a 10×/0.3 Dry lens, 5% laser output using the 488 nm and 639 nm lasers, and a pinhole of 1 AU. Images were processed using ImageJ, where Z-stacks were compressed into one image using maximum intensity and subsequently subtracting the background using a rolling ball algorithm [36]. Subsequently, images were converted to RGB, channels were split to manually count dead (red) and live (green) cells using the ImageJ Cell Counter plugin. Percent viability was determined by dividing the number of live cells by the total number of cells and multiplying by 100%.

2.7. Mechanical testing

For mechanical testing, cylinders (5 mm diameter, 1.4 mm height) were placed on the compression platens of a Bose Electroforce 3220 in an unconfined setup, immersed in PBS, and preloaded with a compressive stress of 2.5 kPa prior to each test. To measure Young's modulus, hydrogels were uniaxially compressed to a strain of 15% at a strain rate of 10 or 16.5% per minute, as indicated. Linear regression was performed on the obtained stress-strain data over the initial 7% of strain [22] to obtain the slope of the initial linear portion of the stress-strain curve (Young's modulus). For creep testing, a 5 kPa stress was applied to the cylinders for 7 min (creep portion) followed by reduction of stress to 2.5 kPa for 7 min (recovery portion). Exponential fitting of the creep and recovery portions of the data was performed using equations (1) and (2) respectively, where $\boldsymbol{\varepsilon}$ represents strain. Note that t corresponds to elapsed time from the moment at which a stress of 5 kPa was reached for equation (1) and the moment at which a stress of 0 Pa was reached for equation (2). a_{creep} and a_{recovery} correspond to the changes in strain caused by creep and recovery respectively while b_{creep} and b_{recovery} correspond to the equilibrium strain values of the creep and

recovery portions respectively. τ is a time constant that corresponds roughly to the amount of time it takes for the strain to reach around 37% of its final value (1/*e*)

$$\varepsilon(t)=a_{\text{creep}}\exp\left(-\frac{t}{\tau_{\text{creep}}}\right)+b_{\text{creep}}, \quad (1)$$

$$\varepsilon(t)=-a_{\text{recovery}}\exp\left(-\frac{t}{\tau_{\text{creep}}}\right)+b_{\text{recovery}}. \quad (2)$$

From the fitting, time-dependent mechanical behavior was quantified using four properties, namely extent of creep, average creep rate, extent of recovery and average recovery rate. The extent of creep is the total change in strain caused by creep while the extent of recovery is the percentage of this strain change that is recovered during unloading. Average creep and recovery rates correspond to the average rates of change in strain over the initial 99% of creep and recovery respectively.

2.8. Swelling kinetics

A swelling kinetics study was performed to assess the impact of microstructural differences on fluid flow. Molded and extruded cylinders (5 mm diameter, 1.4 mm height) were prepared and their exact dimensions (diameter and height) were measured with calipers before they were fully dried. For each cylinder, the polymer density was calculated by dividing the dry weight of the cylinder by the volume of the cylinder obtained from the dimensional measurements. After drying, cylinders were immersed in 10 mL PBS and weighed at multiple time points over 5 days of swelling. Swelling percentage was calculated using equation (3), where M_t corresponds to the hydrogel mass at time t and M_0 corresponds to the initial weight of the dried polymer prior to immersion in PBS

$$\text{Swelling percentage}=\frac{M_t-M_0}{M_0}\times 100\%. \quad (3)$$

2.9. Statistical analysis

Two way-ANOVA with post hoc Tukey analysis was performed to determine statistical significance between groups in the line width vs travel feed rate data and the Young's modulus vs biomaterial composition data. One way-ANOVA with post hoc Tukey analysis was performed to determine statistical significance between groups in the cell viability data. Two-tailed t-tests were performed to compare Young's moduli, creep parameters and polymer density data between extruded and molded cylinders. A two-tailed t-test with Holm-Sidak correction for multiple comparisons was performed on extruded and molded groups in the swelling percentage data. All data are shown as mean ± SEM, with $n = 8$ for all line width data, $n = 5$ for cell viability data and $n = 6$ for all mechanical testing and

swelling data. All graphs were plotted using GraphPad Prism 6 software. A p-value of less than 0.05 was considered statistically significant.

3. Results

3.1. Combinatorial effects of extrusion parameters and biomaterial composition on construct quality and resolution

Qualitative characterization of extruded lines (figure 2) revealed the existence of an optimal extruding pressure at each GelMA concentration investigated (table 1). For each GelMA concentration, extrusion skips were observed at pressures below the optimal range while unevenly excessive outpour was observed above that range.

The impact of printing speed on line resolution was assessed by extruding lines at travel feed rates of 4 mm s^{-1}, 8 mm s^{-1} and 12 mm s^{-1}. The impact of nozzle inner diameter was also evaluated by extruding lines with 27G, 22G and 18G nozzles. As expected, increasing the travel feed rate resulted in a significant decrease in line width, corresponding to an increase in resolution ($p < 0.0001$ for travel feed rate factor in two-way ANOVA), figures 3(a) and (c)) while increasing the inner diameter of the nozzle significantly increased line width ($p < 0.0001$ for one way ANOVA, figures 3(b) and (d)). Interestingly, increasing the GelMA concentration from 10% to 20% w/v also resulted in a small but significant decrease in line width ($p < 0.05$ for GelMA concentration factor in two way ANOVA).

3.2. Cell viability study

To confirm the cytocompatibility of the employed extrusion and photocrosslinking methods, a LIVE/DEAD® assay was performed immediately after the preparation of molded and extruded constructs encapsulated with 3T3 cells. Cell viability was high (~95%) for cells encapsulated in both extruded constructs and molded constructs, as well as for unencapsulated controls, with no significant differences between any of the experimental groups (figure 4). There were no significant differences in cell viability between these three groups and the baseline cell viability measured by Trypan blue exclusion prior to encapsulation and the LIVE/DEAD® assay, which was 97.27% ± 1.12%.

3.3. Impact of extrusion process on bulk mechanical properties

As expected, increasing the GelMA concentration from 10% to 15% and 20% resulted in an increase in the Young's modulus of molded cylinders (figure 5(b)). The concentrations of the photoinitiator (LAP) investigated here had no effect on hydrogel elastic behavior.

The impact of extrusion on Young's modulus was assessed by comparing molded and extruded hydrogel cylinders prepared with 15% GelMA and 0.25% LAP. Surprisingly, while no differences were observed in Young's modulus between molded and extruded cylinders (figure 5(c)), extruded constructs exhibited increased extents (figure 6(b)) and rates of creep (figure 6(c)) compared to molded constructs. Moreover, while the extent of recovery from creep was not different between extruded and molded constructs (figure 6(d)), the rate of recovery from creep was higher for extruded constructs (figure 6(e)). These results indicate

that the extrusion process did not affect bulk elastic behavior (Young's modulus), but time-dependent mechanical behavior was affected.

3.4. Impact of extrusion process on microstructure and swelling properties

To investigate the mechanism behind the observed differences in time-dependent mechanical properties, molded and extruded cylinders were imaged under phase contrast microscopy. Molded constructs were characterized by uniform light transmission through the hydrogel (figure 7(a)) while extruded constructs were characterized by a microstructure with extensive refraction (figure 7(b)). Surprisingly, although extruded and molded hydrogels had similar polymer densities (figure 7(c)) upon fabrication, differences in swelling behavior between extruded and molded constructs were apparent after 1 day, with extruded constructs exhibiting both faster and more extensive swelling compared to molded counterparts (figure 7(d)).

4. Discussion

Our findings show that the bioprinting process results in hydrogels with unique microstructures that differ from their molded counterparts prepared with the same polymer solution and with the same dimensions, causing major changes in time-dependent mechanical properties and swelling behavior. These results have major implications for the design of hydrogels for biomedical applications in which the hydrogels would be required to withstand mechanical loading *in vivo*.

The identification of optimal extrusion pressures and the observed increase in resolution with printing speed and nozzle gauge are consistent with previous characterizations of extrusion-based methods [37–39]. The impact of GelMA concentration on Young's modulus is also in agreement with previous studies performed with other photoinitiators [18]. However, the unexpected impact of GelMA concentration on resolution, very likely the result of increased flow resistance due to the concomitant rise of hydrogel viscosity with polymer concentration, reveals yet another mechanism at play in the determination of printing specifications. The fact that the extrusion process did not affect cell viability is in agreement with previous reports that allowing hydrogel solutions to undergo gelation prior to extrusion protects encapsulated cells from the detrimental effects of extrusion-induced shear forces [40].

More interesting is the finding that the extrusion process impacts the time-dependent mechanical behavior of hydrogel constructs. The fact that swelling kinetics between molded and extruded hydrogels were different, despite similar densities, suggest that microstructural differences contribute to the observed differences. Indeed, the interstices present in the microstructure of the extruded construct constitute an interconnected network of space available to the surrounding medium, thereby increasing the rate and extent of fluid flow both into and out of the construct during loading and unloading. The differences in mechanical behavior of the extruded and molded constructs would be expected to be even greater after the hydrogels reached swelling equilibrium, which should be studied in future work. It is also possible that spatial differences in crosslinking existed because the first printed layers were exposed to the light source for longer periods of time than the last

printed layers. However, because molded and extruded hydrogels did not show differences in elastic moduli, any spatial differences in crosslinking were likely too minor to affect mechanical properties. Finally, it is possible that lateral translation of the potentially unconstrained structural filaments with respect to each other may constitute another mechanism by which extrusion increases the rate and extent of creep. However, our finding that the extent of recovery is identical in extruded and molded constructs suggests similar extents of permanent deformation. Clearly, further studies are warranted to thoroughly investigate the effects of the extrusion process on the microstructure and mechanical properties of hydrogels.

The reported mechanical results have important implications both for *in vitro* tissue development and for *in vivo* settings following implantation. Firstly, native tissues also exhibit time-varying mechanical properties [41–44], so it is essential to understand how hydrogels behave in comparison in order to better design biomimetic constructs. Moreover, it has also been shown that cells respond differently to varying substrate stiffness in terms of morphology [45], movement [46] and differentiation [47], so it stands to reason that cell behavior will also be affected by viscoelastic substrate properties. On the other hand, cells may respond more to local changes in mechanical properties on the nano- or micro-scale compared to changes in bulk mechanical properties that were evaluated in this study. Nonetheless, the preponderance of studies establishing mechanical stimulation as a key regulator in native biological processes, such as gene transcription [48], tissue morphogenesis [49], neural transduction [50], cell–cell junction signaling [51], and tissue development [52, 53], highlight the importance of understanding the response of cell-laden hydrogels to mechanical loading [54–56]. Our findings that the bioprinting process also affects swelling behavior are likewise pertinent to biomedical applications as swelling behavior mediates changes in volume and concentration upon implantation into the osmotic environment of the body [57]. Accordingly, the effects of swelling properties may need to be curbed by preconditioning to prevent failure [57–59] or may be exploited for the development of smart biomaterials [60]. Taken together, our findings suggest that a more comprehensive characterization of bioprinted constructs must be conducted in order to systematically predict and monitor properties that are vital to their performance.

Time-dependent mechanical properties of extruded highly porous scaffolds have previously been evaluated, most notably with stress relaxation testing [61, 62]. These studies, however, solely assess the impact of intended scaffold porosity rather than the unintended impact of the extrusion process itself on the mechanical behavior of constructs. Similarly, previous swelling studies performed on extruded constructs [63] overlook the impact of extrusion as they lack comparisons against molded counterparts. Interestingly, it was previously shown that the swelling behavior of constructs fabricated with inkjet printing is not different from that of nonprinted hydrogels [64]. Given that inkjet printing dispenses liquid droplets that form a series of consolidated layers devoid of unintended discontinuities [65], these results serve to confirm our finding that interstices formed during extrusion are responsible for the observed differences in swelling behavior. However, further studies are required to thoroughly characterize the microstructure of extruded and molded hydrogels.

This study did have several limitations. Firstly, the only biomaterial evaluated was gelatin methacrylate. Although this material is widely used in tissue engineering [18], the results may differ for other bioinks, including collagen [66], hyaluronic acid [67] and alginate [68], as well as other crosslinking methods such as physical or ionic crosslinking. In addition, this study only evaluated one composition of gelatin hydrogel in extruded and molded forms under just two mechanical testing scenarios. Future studies should include multiple time-dependent mechanical testing protocols for varying bioprinting parameters, namely extrusion speed and nozzle diameter, as well as for constructs with different biomaterial formulations, all of which are likely to affect transient and equilibrium loading responses. Moreover, although our goal in this study was to compare the properties of extruded and molded hydrogels immediately after fabrication, mechanical characterization after the hydrogels reach swelling equilibrium also will be important for their intended applications. Nanoindentation studies may be more relevant tests to determine how encapsulated cells might respond to changes in mechanical behavior [69]. Swelling studies should be conducted using osmotic solutions that more accurately recapitulate the intended application, as PBS has been shown to be a poor indicator of the high osmotic pressures found in many tissues *in vivo* [57]. Finally, we were not able to thoroughly characterize the microstructure of the hydrogel constructs, considering most methods of porosimetry require gel dehydration, which would affect the microstructure of the gels [22]. Future studies should be directed at characterizing differences in microstructure due to the extrusion process. Nonetheless, the current study constitutes a concrete step towards the systematic and comprehensive evaluation of the impact of both biomaterial formulation and the extrusion process on construct properties, most notably mechanical properties.

5. Conclusions

The current study builds on the growing body of bioprinting characterization studies, a collective that sheds light on an intricate interplay between printing parameters and construct properties. Of particular significance is the study's finding that extrusion creates a microstructure that increases the extent and rate of both swelling and creep compared to molded counterparts. This important process may be exploited, mitigated, or otherwise addressed in the design of extruded hydrogels used for biomedical applications. Indeed, both swelling and time-dependent mechanical behavior greatly impact the success of hydrogels used in tissue engineering and *in vivo* implantation.

Acknowledgments

The authors gratefully acknowledge the Cell Imaging Center at Drexel University as well as technical assistance from Ricardo Solorzano, Daniel Cabrera, Victoria Leon, Hannah Geisler, Austin Philip, Brandon Marcinkiewicz, and Dolores Conover. The authors also thank Dr Sriram Balasubramanian for helpful discussions.

References

1. Shafran D, Kodish E, Tzakis A. Organ shortage: the greatest challenge facing transplant medicine. World J Surg. 2014; 38:1650–7. [PubMed: 24831673]
2. Hoffman AS. Hydrogels for biomedical applications. Adv Drug Deliv Rev. 2012; 64:18–23.
3. Nicodemus GD, Bryant SJ. Cell encapsulation in biodegradable hydrogels for tissue engineering applications. Tissue Eng B: Rev. 2008; 14:149–65.

4. Yoon J, Cai S, Suo Z, Hayward RC. Poroelastic swelling kinetics of thin hydrogel layers: comparison of theory and experiment. Soft Matter. 2010; 6:6004–12.
5. Vaughan BL, Galie PA, Stegemann JP, Grotberg JB. A poroelastic model describing nutrient transport and cell stresses within a cyclically strained collagen hydrogel. Biophys J. 2013; 105:2188–98. [PubMed: 24209865]
6. Chen DT, Wen Q, Janmey PA, Crocker JC, Yodh AG. Rheology of soft materials. Condens Matter Phys. 2010; 1:301–22.
7. Doi, M.; Edwards, SF. The theory of polymer dynamics. Vol. 73. Oxford: Clarendon Press; 1988.
8. Mandrycky C, Wang Z, Kim DH, Kim K. 3D bioprinting for engineering complex tissues. Biotechnol Adv. 2016; 34:422–34. [PubMed: 26724184]
9. Murphy SV, Atala A. 3D bioprinting of tissues and organs. Nat Biotechnol. 2014; 32:773–85. [PubMed: 25093879]
10. Ozbolat IT, Hospodiuk M. Current advances and future perspectives in extrusion-based bioprinting. Biomaterials. 2016; 76:321–43. [PubMed: 26561931]
11. Chang CC, Boland ED, Williams SK, Hoying JB. Direct-write bioprinting three-dimensional biohybrid systems for future regenerative therapies. J Biomed Mater Res B: Appl Biomater. 2011; 98:160–70. [PubMed: 21504055]
12. Boland T, Mironov V, Gutowska A, Roth E, Markwald RR. Cell and organ printing: II. Fusion of cell aggregates in three-dimensional gels. Anatomical Rec A: Discoveries Mol Cell Evolutionary Biol. 2003; 272:497–502.
13. Skardal A, Atala A. Biomaterials for integration with 3D bioprinting. Ann Biomed Eng. 2015; 43:730–46. [PubMed: 25476164]
14. Song SJ, Choi J, Park YD, Lee JJ, Hong SY, Sun K. A three-dimensional bioprinting system for use with a hydrogel-based biomaterial and printing parameter characterization. Artif Organs. 2010; 34:1044–8. [PubMed: 21092048]
15. Song SJ, Choi J, Park YD, Hong S, Lee JJ, Ahn CB, Choi H, Sun K. Sodium alginate hydrogel-based bioprinting using a novel multinozzle bioprinting system. Artif Organs. 2011; 35:1132–6. [PubMed: 22097985]
16. Sawkins MJ, Mistry P, Brown BN, Shakesheff KM, Bonassar LJ, Yang J. Cell and protein compatible 3D bioprinting of mechanically strong constructs for bone repair. Biofabrication. 2015; 7:035004. [PubMed: 26133398]
17. Schuurman W, Khristov V, Pot M, Van Weeren P, Dhert W, Malda J. Bioprinting of hybrid tissue constructs with tailorable mechanical properties. Biofabrication. 2011; 3:021001. [PubMed: 21597163]
18. Schuurman W, Levett PA, Pot MW, van Weeren PR, Dhert WJ, Hutmacher DW, Melchels FP, Klein TJ, Malda J. Gelatin-methacrylamide hydrogels as potential biomaterials for fabrication of tissue-engineered cartilage constructs. Macromol Biosci. 2013; 13:551–61. [PubMed: 23420700]
19. Zhang T, Yan KC, Ouyang L, Sun W. Mechanical characterization of bioprinted in vitro soft tissue models. Biofabrication. 2013; 5:045010. [PubMed: 24280635]
20. Ganji F, Vasheghani-Farahani S, Vasheghani-Farahani E. Theoretical description of hydrogel swelling: a review. Iran Polym J. 2010; 19:375–98.
21. Evmenenko G, Budtova T. Structural changes in hydrogels immersed in a linear polymer solution, studied by SANS. Polymer. 2000; 41:4943–7.
22. Spiller KL, Laurencin SJ, Charlton D, Maher SA, Lowman AM. Superporous hydrogels for cartilage repair: evaluation of the morphological and mechanical properties. Acta Biomaterialia. 2008; 4:17–25. [PubMed: 18029236]
23. Koetting MC, Peters JT, Steichen SD, Peppas NA. Stimulus-responsive hydrogels: theory, modern advances, and applications. Mater Sci Eng: R: Rep. 2015; 93:1–49. [PubMed: 27134415]
24. Sannino A, Madaghiele M, Conversano F, Mele G, Maffezzoli A, Netti P, Ambrosio L, Nicolais L. Cellulose derivative-hyaluronic acid-based microporous hydrogels cross-linked through divinyl sulfone (DVS) to modulate equilibrium sorption capacity and network stability. Biomacromolecules. 2004; 5:92–6. [PubMed: 14715013]

25. Nichol JW, Koshy ST, Bae H, Hwang CM, Yamanlar S, Khademhosseini A. Cell-laden microengineered gelatin methacrylate hydrogels. Biomaterials. 2010; 31:5536–44. [PubMed: 20417964]
26. Kolesky DB, Truby RL, Gladman A, Busbee TA, Homan KA, Lewis JA. 3D bioprinting of vascularized, heterogeneous cell-laden tissue constructs. Adv Mater. 2014; 26:3124–30. [PubMed: 24550124]
27. Shin H, Olsen BD, Khademhosseini A. The mechanical properties and cytotoxicity of cell-laden double-network hydrogels based on photocrosslinkable gelatin and gellan gum biomacromolecules. Biomaterials. 2012; 33:3143–52. [PubMed: 22265786]
28. Billiet T, Gevaert E, DeSchryver T, Cornelissen M, Dubruel P. The 3D printing of gelatin methacrylamide cell-laden tissue-engineered constructs with high cell viability. Biomaterials. 2014; 35:49–62. [PubMed: 24112804]
29. Liu K, Ovaert TC. Poroviscoelastic constitutive modeling of unconfined creep of hydrogels using finite element analysis with integrated optimization method. J Mech Behav Biomed Mater. 2011; 4:440–50. [PubMed: 21316632]
30. Silva P, Crozier S, Veidt M, Pearcy MJ. An experimental and finite element poroelastic creep response analysis of an intervertebral hydrogel disc model in axial compression. J Mater Sci, Mater Med. 2005; 16:663–9. [PubMed: 15965599]
31. Oyen M. Mechanical characterisation of hydrogel materials. Int Mater Rev. 2014; 59:44–59.
32. Fairbanks BD, Schwartz MP, Bowman CN, Anseth KS. Photoinitiated polymerization of PEG-diacrylate with lithium phenyl-2, 4, 6-trimethylbenzoylphosphinate: polymerization rate and cytocompatibility. Biomaterials. 2009; 30:6702–7. [PubMed: 19783300]
33. Lin H, Zhang D, Alexander PG, Yang G, Tan J, Cheng AWM, Tuan RS. Application of visible light-based projection stereolithography for live cell-scaffold fabrication with designed architecture. Biomaterials. 2013; 34:331–9. [PubMed: 23092861]
34. Preibisch S, Saalfeld S, Tomancak P. Globally optimal stitching of tiled 3D microscopic image acquisitions. Bioinformatics. 2009; 25:1463–5. [PubMed: 19346324]
35. Benedikt S, Wang J, Markovic M, Moszner N, Dietliker K, Ovsianikov A, Grützmacher H, Liska R. Highly efficient water-soluble visible light photoinitiators. J Polym Sci A. 2016; 54:473–9.
36. Sternberg SR. Biomedical image processing. Computer. 1983; 16:22–34.
37. Domingos M, Chiellini F, Gloria A, Ambrosio L, Bartolo P, Chiellini E. Effect of process parameters on the morphological and mechanical properties of 3D bioextruded poly (ε-caprolactone) scaffolds. Rapid Prototyping J. 2012; 18:56–67.
38. Iwami, K.; Umeda, N. Rapid Prototyping in Biomedical Engineering. In: Hoque, ME., editor. Advanced Applications of Rapid Prototyping Technology in Modern Engineering. Rijeka: InTech; 2011. p. 75-90.
39. Fedorovich NE, Schuurman W, Wijnberg HM, Prins HJ, van Weeren PR, Malda J, Alblas J, Dhert WJ. Biofabrication of osteochondral tissue equivalents by printing topologically defined, cell-laden hydrogel scaffolds. Tissue Eng C: Methods. 2011; 18:33–44.
40. Aguado BA, Mulyasasmita W, Su J, Lampe KJ, Heilshorn SC. Improving viability of stem cells during syringe needle flow through the design of hydrogel cell carriers. Tissue Eng A. 2011; 18:806–15.
41. Evans DW, Moran EC, Baptista PM, Soker S, Sparks JL. Scale-dependent mechanical properties of native and decellularized liver tissue. Biomech Model Mechanobiol. 2013; 12:569–80. [PubMed: 22890366]
42. Keenan KE, Pal S, Lindsey DP, Besier TF, Beaupre GS. A viscoelastic constitutive model can accurately represent entire creep indentation tests of human patella cartilage. J Appl Biomech. 2013; 29:292. [PubMed: 23027200]
43. Budday S, Nay R, deRooij R, Steinmann P, Wyrobek T, Ovaert TC, Kuhl E. Mechanical properties of gray and white matter brain tissue by indentation. J Mech Behav Biomed Mater. 2015; 46:318–30. [PubMed: 25819199]
44. Deeb, G.; Hasan, A.; Abiad, M.; Alhadrami, HA.; Mustafy, T. 2015 Int Conf on Advances in Biomedical Engineering (ICABME). Piscataway, NJ: IEEE; 2015. Experimental studies and

computer modeling of viscoelastic properties of heart valve leaflets: implication in heart valve tissue engineering; p. 226-9.

45. Yeung T, Georges PC, Flanagan LA, Marg B, Ortiz M, Funaki M, Zahir N, Ming W, Weaver V, Janmey PA. Effects of substrate stiffness on cell morphology, cytoskeletal structure, and adhesion. Cell Motil Cytoskeleton. 2005; 60:24–34. [PubMed: 15573414]
46. Lo CM, Wang HB, Dembo M, Wang Yl. Cell movement is guided by the rigidity of the substrate. Biophys J. 2000; 79:144–52. [PubMed: 10866943]
47. Engler AJ, Sen S, Sweeney HL, Discher DE. Matrix elasticity directs stem cell lineage specification. Cell. 2006; 126:677–89. [PubMed: 16923388]
48. Mammoto A, Mammoto T, Ingber DE. Mechanosensitive mechanisms in transcriptional regulation. J Cell Sci. 2012; 125:3061–73. [PubMed: 22797927]
49. Lecuit T, Lenne PF, Munro E. Force generation, transmission, and integration during cell and tissue morphogenesis. Annu Rev Cell Developmental Biol. 2011; 27:157–84.
50. Cheng CM, Lin YW, Bellin RM, Steward RL, Cheng YR, LeDuc PR, Chen CC. Probing localized neural mechanotransduction through surface-modified elastomeric matrices and electrophysiology. Nat Protocol. 2010; 5:714–24.
51. Huveneers S, de Rooij J. Mechanosensitive systems at the cadherin–F-actin interface. J Cell Sci. 2013; 126:403–13. [PubMed: 23524998]
52. Hilz FM, Ahrens P, Grad S, Stoddart MJ, Dahmani C, Wilken FL, Sauerschnig M, Niemeyer P, Zwingmann J, Burgkart R. Influence of extremely low frequency, low energy electromagnetic fields and combined mechanical stimulation on chondrocytes in 3-D constructs for cartilage tissue engineering. Bioelectromagnetics. 2014; 35:116–28. [PubMed: 24203577]
53. Morgan KY, Black LD III. Mimicking isovolumic contraction with combined electromechanical stimulation improves the development of engineered cardiac constructs. Tissue Eng A. 2014; 20:1654–67.
54. Egan P, Sinko R, LeDuc PR, Keten S. The role of mechanics in biological and bio-inspired systems. Nat Commun. 2015; 6:7418–29. [PubMed: 26145480]
55. Guilak F, Butler DL, Goldstein SA, Baaijens FP. Biomechanics and mechanobiology in functional tissue engineering. J Biomech. 2014; 47:1933–40. [PubMed: 24818797]
56. Hasan A, Ragaert K, Swieszkowski W, Selimović Š, Paul A, Camci-Unal G, Mofrad MR, Khademhosseini A. Biomechanical properties of native and tissue engineered heart valve constructs. J Biomech. 2014; 47:1949–63. [PubMed: 24290137]
57. Spiller KL, Laurencin SJ, Lowman AM. Characterization of the behavior of porous hydrogels in model osmotically-conditioned articular cartilage systems. J Biomedi Mater Res B: Appl Biomater. 2009; 90:752–9.
58. Heilmann S, Küchler S, Wischke C, Lendlein A, Stein C, Schäfer-Korting M. A thermosensitive morphine-containing hydrogel for the treatment of large-scale skin wounds. Int J Pharmaceutics. 2013; 444:96–102.
59. Ciolino JB, Stefanescu CF, Ross AE, Salvador-Culla B, Cortez P, Ford EM, Wymbs KA, Sprague SL, Mascoop DR, Rudina SS. In vivo performance of a drug-eluting contact lens to treat glaucoma for a month. Biomaterials. 2014; 35:432–9. [PubMed: 24094935]
60. Chang C, Duan B, Cai J, Zhang L. Superabsorbent hydrogels based on cellulose for smart swelling and controllable delivery. Eur Polym J. 2010; 46:92–100.
61. Yousefi AM, Gauvin C, Sun L, DiRaddo RW, Fernandes J. Design and fabrication of 3D-plotted polymeric scaffolds in functional tissue engineering. Polym Eng Sci. 2007; 47:608–18.
62. El-Ayoubi R, DeGrandpré C, DiRaddo R, Yousefi AM, Lavigne P. Design and dynamic culture of 3D-scaffolds for cartilage tissue engineering. J Biomater Appl. 2011; 25:429–44. [PubMed: 20042429]
63. Loozen LD, Wegman F, #x000D6;ner FC, Dhert WJ, Alblas J. Porous bioprinted constructs in BMP-2 non-viral gene therapy for bone tissue engineering. J Mater Chem B. 2013; 1:6619–26.
64. Cui X, Breitenkamp K, Finn M, Lotz M, D'Lima DD. Direct human cartilage repair using three-dimensional bioprinting technology. Tissue Eng A. 2012; 18:1304–12.
65. Saunders RE, Derby B. Inkjet printing biomaterials for tissue engineering: bioprinting. Int Mater Rev. 2014; 59:430–48.

66. Glowacki J, Mizuno S. Collagen scaffolds for tissue engineering. Biopolymers. 2008; 89:338–44. [PubMed: 17941007]

67. Collins MN, Birkinshaw C. Hyaluronic acid based scaffolds for tissue engineering—a review. Carbohydrate Polym. 2013; 92:1262–79.

68. Sun J, Tan H. Alginate-based biomaterials for regenerative medicine applications. Materials. 2013; 6:1285–309.

69. Oyen ML. Nanoindentation of hydrated materials and tissues. Curr Opin Solid State Mater Sci. 2015; 19:317–23.

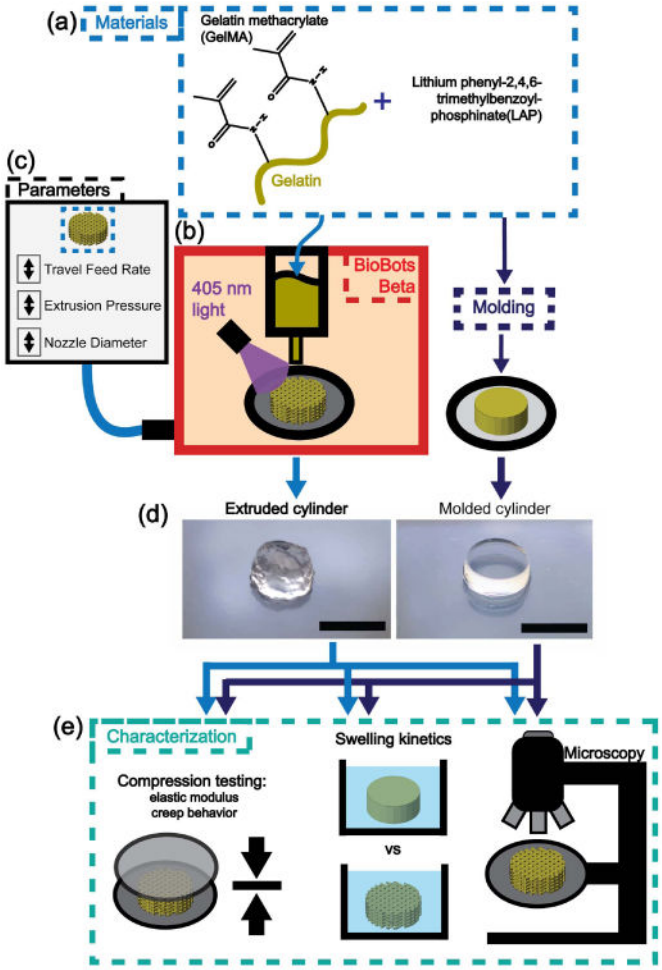

Figure 1.

Experimental design. (a) Various formulations of gelatin methacrylate (GelMA) hydrogel photocrosslinked with lithium phenyl-2,4,6-trimethylbenzoylphosphinate (LAP) were extruded into different structures (b) at varying travel feed rates, nozzle diameters and extrusion pressures (c). (d) Hydrogels with the same dimensions were prepared, and (e) hydrated unconfined compression testing, a swelling study, and optical microscopy were used to evaluate construct properties for comparison against molded counterparts prepared with the exact same dimensions. Scale bars: 5 mm.

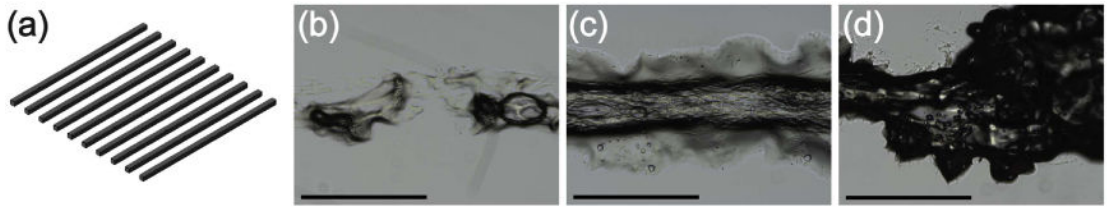

Figure 2.

Optimal extruding pressure is dependent on biomaterial composition. (a) Sequential lines, as shown by CAD model, were extruded at various concentrations (10%, 15% and 20% w/v GelMA) and pressures (0–140 psi) with a 27G nozzle. LAP concentration was 0.5% w/v and travel feed rate was 8 mm s^{-1}. Micrographs shown are representative of line extrusions at 60 psi (b), 80 psi (c) and 100 psi (d) for 10% GelMA/0.25% LAP. Scale bars: 1000 μm.

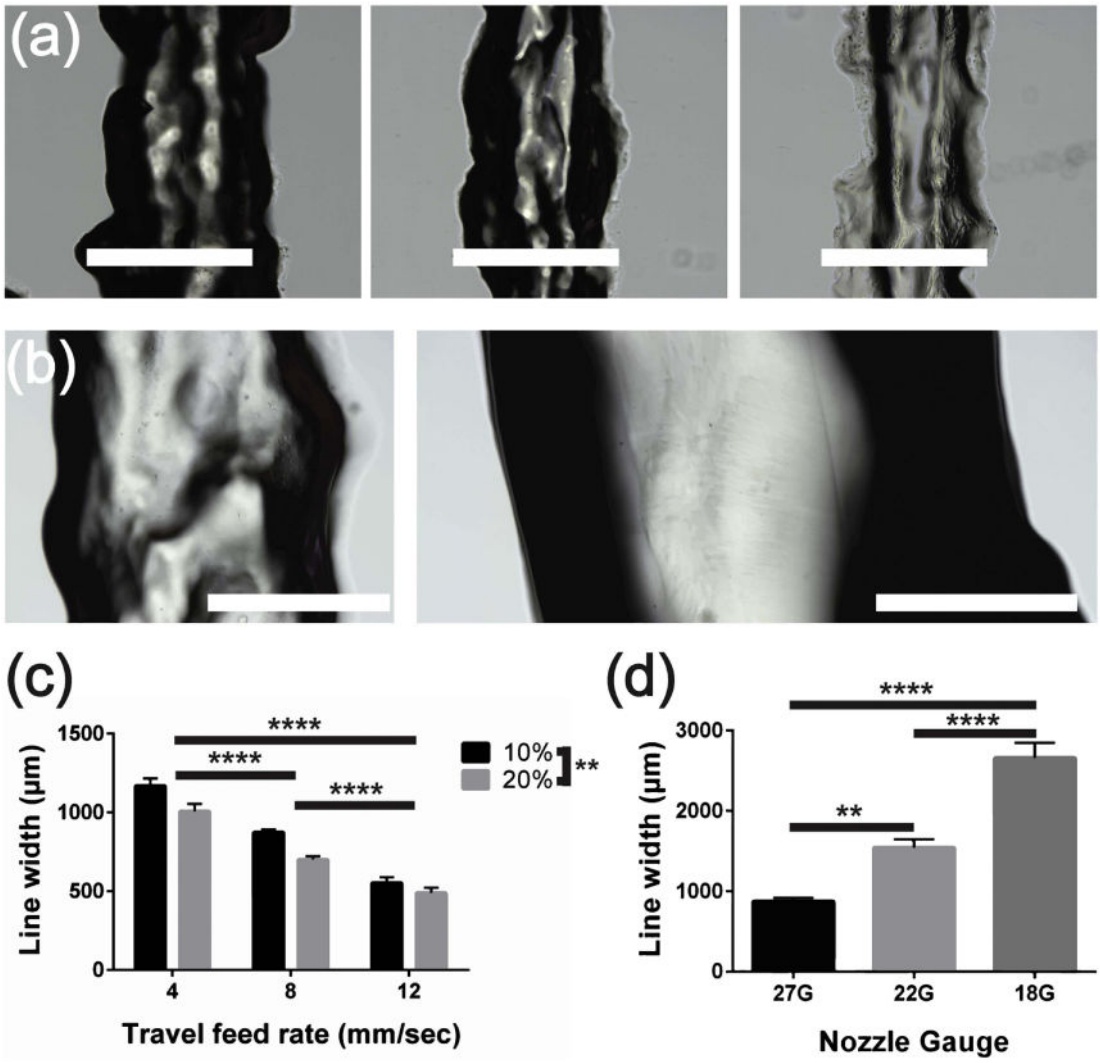

Figure 3.

Both travel feed rate and biomaterial composition modulate extrusion resolution, measured by line thickness. (a) Representative images shown for line extrusions at 4 mm s^{-1} (left), 8 mm s^{-1} (center) and 12 mm s^{-1} (right) for 10% GelMA/0.25% LAP. Scale bars: 1000 μm. (b) Representative images shown for line extrusions with a 22G nozzle at the optimal pressure of 40 psi (left) and with an 18G nozzle at the optimal pressure of 10 psi (right) for 10% GelMA/0.25% LAP and a travel feed rate of 8 mm s^{-1}. Scale bars: 1000 μm. (c) Line thickness data as a function of GelMA concentration (10% or 20%) and travel feed rate, quantified by micrograph analysis (****$p \leq 0.0001$, two way ANOVA and Tukey post hoc analysis). (d) Line thickness data as a function of nozzle gauge quantified by micrograph analysis (**$p \leq 0.01$,****$p \leq 0.0001$, one way ANOVA and Tukey post hoc analysis).

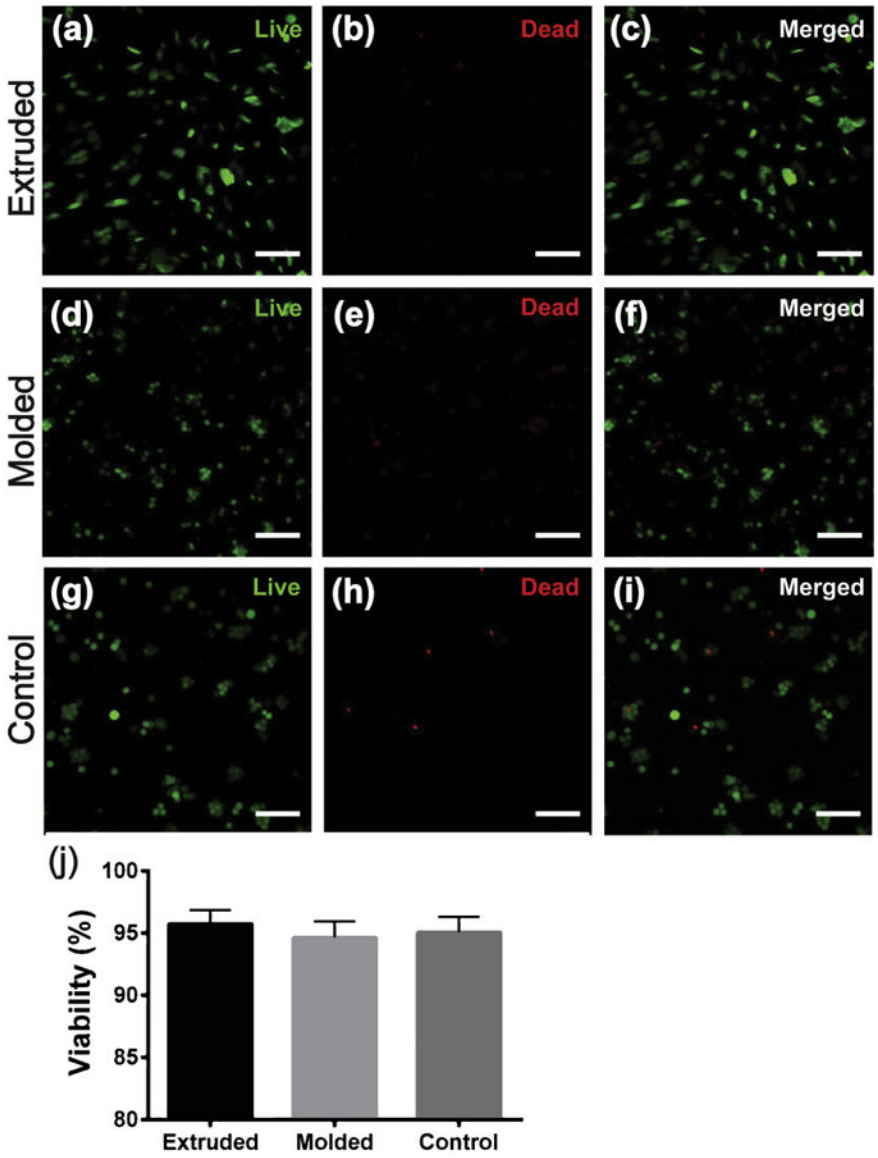

Figure 4.

Cell viability was not affected by 3D printing process. (a)–(c) 3D printed hydrogel lines; (d)–(f) molded hydrogels; (g)–(i) cell-only controls. (j) Quantitative analysis of cell viability. Scale bars are 100 μm.

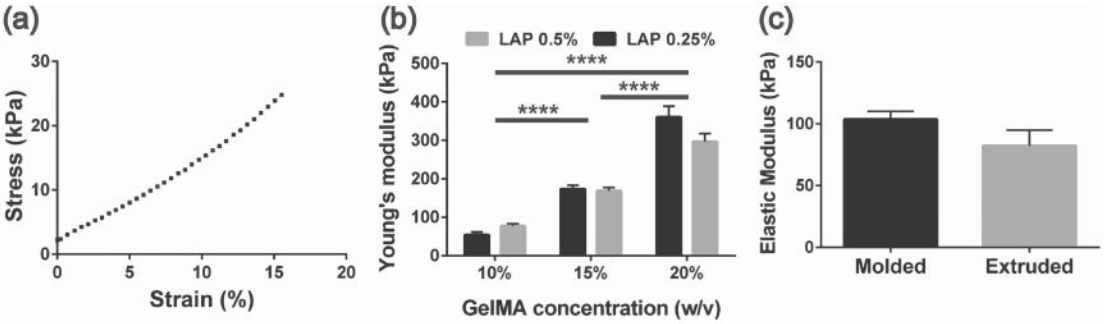

Figure 5.

Elastic deformation behavior is modulated by biomaterial composition but not by printing itself. (a) Representative portion of stress/strain data from unconfined compression. (b) Young's moduli of hydrogels prepared with 10%, 15%, 20% GelMA and 0.25%, 0.5% LAP (****$p \leq 0.0001$). There was no significant difference between hydrogels prepared with 0.25% and 0.5% LAP. (c) Young's moduli of printed and molded GelMA cylinders (15% GelMA, 0.25% LAP). Note that elastic moduli in (b) were measured in uniaxial compression with a strain rate of 10%/min, while elastic moduli in (c) were measured using a strain rate of 16.5%/min.

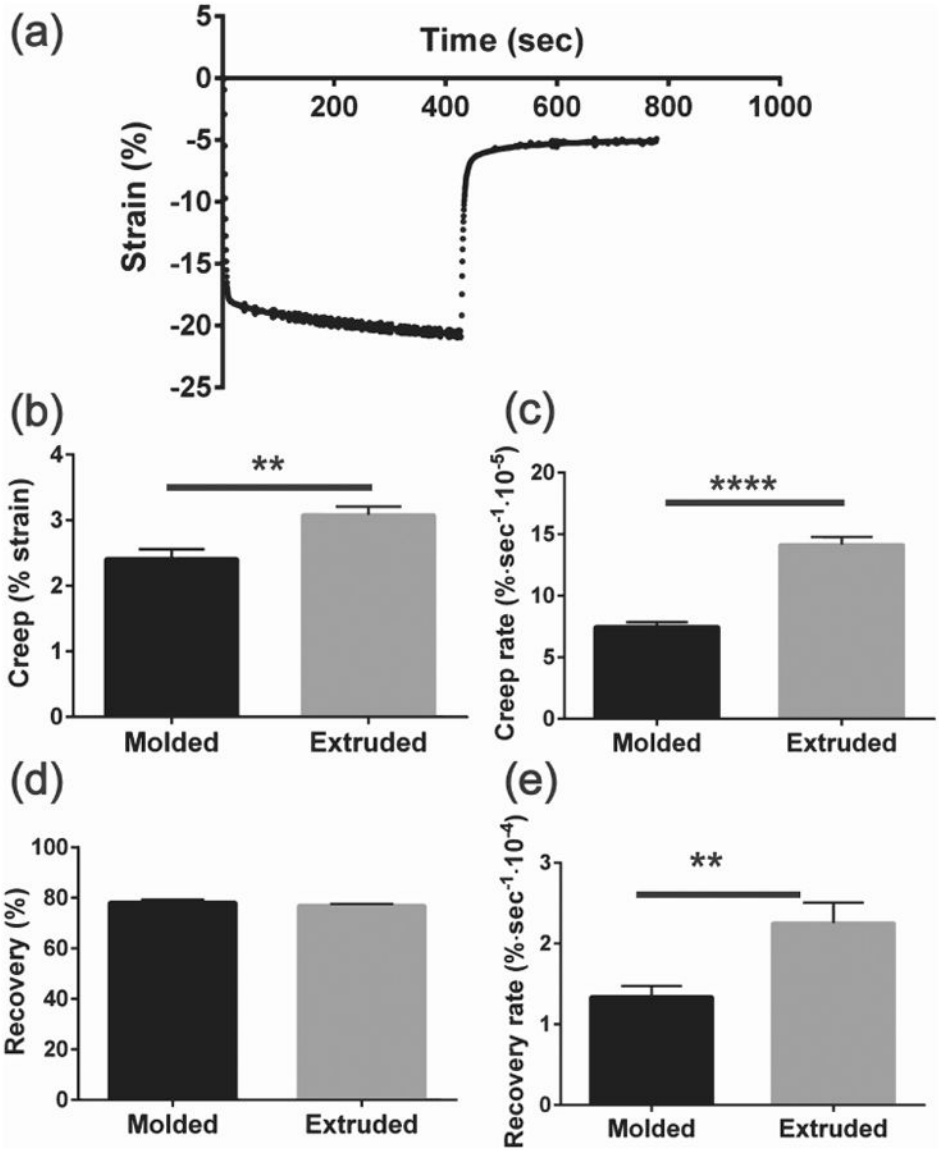

Figure 6.

Printing affects rate and extent of time-dependent mechanical behavior. Printed and molded GelMA cylinders (15% GelMA, 0.25% LAP) were subjected to creep testing in hydrated unconfined compression. (a) Representative strain vs time data shown for creep + recovery testing of printed cylinders. (b) Creep extent data, obtained from exponential regression of creep portion (** $p < 0.01$). (c) Creep rate data, obtained from exponential regression of creep portion (**** $p < 0.0001$). (d) Recovery extent data, obtained from exponential regression of recovery portion. (e) Recovery rate data, obtained from exponential regression of recovery portion (** $p < 0.01$).

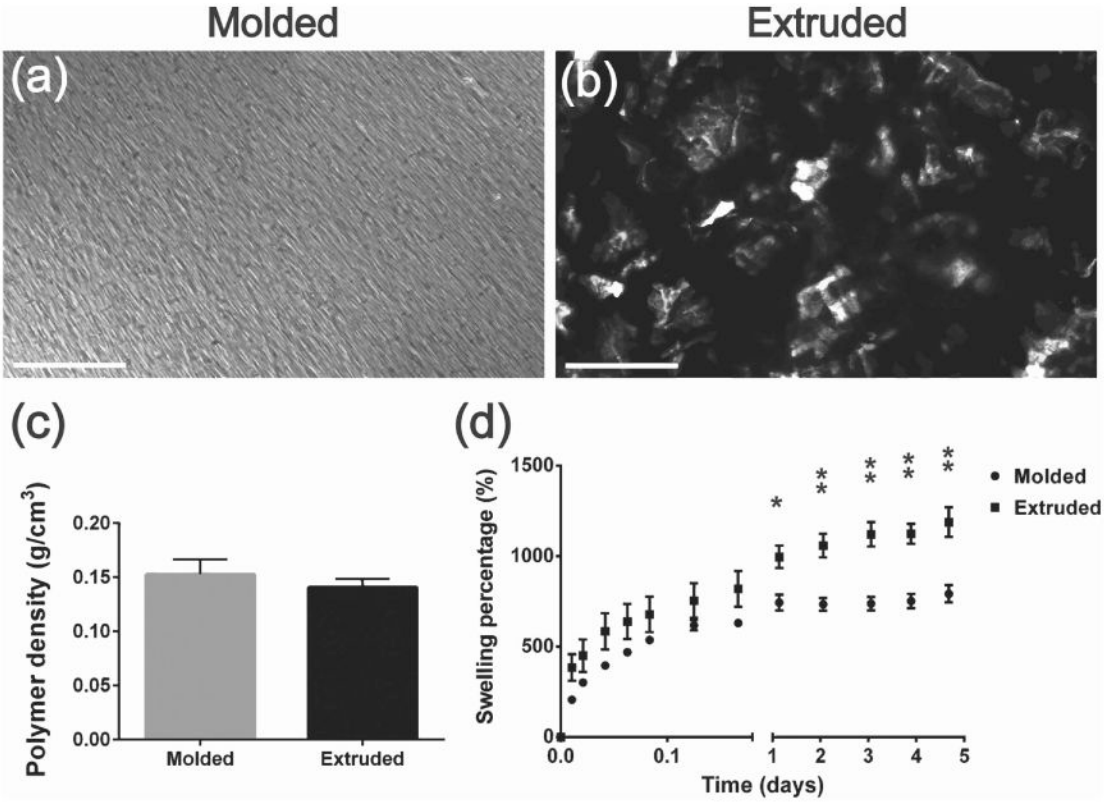

Figure 7.

Printed and molded hydrogels exhibit different microstructures as well as swelling behavior. Optical micrographs for molded (a) and printed (b) GelMA samples (15% GelMA, 0.25% LAP). Scale bars: 500 μm. (c) Polymer density of extruded and molded cylinders. No statistical difference between the two groups. (d) Swelling percentage data (*$p < 0.05$, **$p < 0.01$) obtained from weighing printed and molded GelMA cylinders (15% GelMA, 0.25% LAP) over time in immersion in PBS.

Table 1

Qualitative characterization of line extrusions (with a 27G nozzle and a travel feed rate of 8 mm s^{-1}) reveals the existence of optimal GelMA concentration/extrusion pressure pairings.

	Characteristics of printed lines		
GelMA concentration	**Noncontinuous flow, uneven thickness: beads instead of lines**	**Optimal pressure, continuous flow, constant thickness**	**Excessive outpour, uneven thickness, large chunks in lines**
10% w/v GelMA	60 psi	80 psi	100 psi
15% w/v GelMA	80 psi	100–110 psi	120 psi
20% w/v GelMA	100 psi	130 psi	—[a]

[a]Required extrusion pressure exceeded the capabilities of the extruder.